Microchimica Acta
https://doi.org/10.1007/s00604-019-3811-0

ORIGINAL PAPER

Gold nanoparticle-based signal enhancement of an aptasensor for ractopamine using liquid crystal based optical imaging

Ying Wang[1,2] · Bing Wang[3] · XingLiang Xiong[2] · ShiXiong Deng[2]

Received: 23 April 2019 / Accepted: 9 September 2019

Abstract

The authors report on a method for the determination of ractopamine (RAC) via liquid crystal (LC) optical imaging and gold nanoparticle-induced signal enhancement. The gold nanoparticles (AuNPs) were blended with the desired concentrations of RAC, and this is found to strongly improve the performance of the assay. The RAC aptamers were immobilized on the self-assembled film of a glass slide for specific recognition of RAC. This causes a homeotropic re-orientation of the LCs. Notably, the aptamers need not be immobilized on the nanoparticles like in other methods. The addition of RAC causes the formation of an AuNP-RAC-aptamer conjugate on the sensing interface. This disrupts the orientation of LCs and results in a change of the polarized images of the LCs. The method has a detection limit as low as 1 pM of RAC.

Keywords Aptamer · Biosensor · Self-assembled film · Glass slide · Recognition · Conjugate · Sensing interface · Orientation · Polarized image · Homeotropic re-orientation

Introduction

Ractopamine (RAC) is a synthetic β-adrenergic agonist which is often used as a drug to treat human respiratory diseases [1]. It is also widely used as nutrient agent in animals to enhance the muscle tissues production [2]. However, RAC can be residues in animal tissues and eventually become enriched after entering the human body through the food chain which will generate some detrimental side effects such as headache, nervousness, nausea, muscle tremors, and tachycardia [3, 4]. Although, RAC has been banned for animal feed additives in many countries [5], driven by profits, RAC are still being used in large quantities. It is urgent and important to develop a sensitive and rapid technology of detecting RAC. Up to now, a lot of analytical methods have been applied for the detection of RAC, including gas chromatography–mass spectrometry [6], liquid chromatography-mass spectrometry [7–9], immunoassay [10], capillary electrophoresis [11], and chemiluminescence [12]. Nevertheless, some of the above techniques also exhibit some disadvantages. For example, they are expensive, time-consuming and have tedious pretreatment procedures.

Two approaches are usually adopted to improve the detection sensitivity. One way is to use the instrument for the signal enhancement. This method usually needs the use of large expensive instruments and requires tedious pre-treatment and professionals, resulting in high detection costs. The other approach is the use of a biotin-avidin system combined with nanomaterials, but this method generally requires complex preparation procedure, leading to problems such as low repeatability of the detection method. Abbott proposed a liquid crystals (LCs) biosensor which can detect biochemical binding events on sensor surfaces by using of the inherent natural signal amplification of LCs [13, 14]. LCs own many unique characteristics, such as sensitive orientation response, elastic strain and birefringence [15]. Minute changes of the substrate surface can be smartly sensed

Electronic supplementary material The online version of this article (https://doi.org/10.1007/s00604-019-3811-0) contains supplementary material, which is available to authorized users.

✉ XingLiang Xiong
xiongxingliang7212@163.com

✉ ShiXiong Deng
dengshixiong1963@163.com

Ying Wang
wendy8657@163.com

[1] School of Medical Information Engineering, Jining Medical University, Rizhao 276826, Shandong, China

[2] Laboratory of Biomedical Engineering, Chongqing Medical University, Chongqing 400016, China

[3] Hospital of Traditional Chinese Medicine in Rizhao City, Rizhao 276800, China

Published online: 15 October 2019

by LCs due to their sensitive orientation response. Then the response of LCs will be naturally amplified into the bulk LC film for macroscopic distances because of their elastic strain. This amplified response is further transduced into the changes of optical appearance through a crossed polarizer due to the birefringence of LCs, which can be observed visually. Therefore, LC is a very good molecular recognition element for signal transduction and amplification.

Aptamer-based liquid crystal biosensors which are called LC aptasensors have been widely developed as a sensing platform for detecting proteins, oligonucleotides and small inorganic molecules [16–18]. Aptamers are single-stranded DNA/RNA molecules selected for their high affinity and selectivity for the target molecules including small molecules, drugs, inorganic ions proteins, and even cells [19]. In these LC assays, aptamers act as molecular recognition probes which can be immobilized on the sensing interface. These LC assays share the common advantages of LCs and aptamers.

Gold nanoparticles (AuNPs) have unique chemical and physical properties, including good biocompatibility, easy preparation and their large surface areas [20, 21]. Consequently, AuNPs can be applied for the fabrication of various biological and chemical systems [22]. It has been reported that many organic compounds containing electron-rich groups can be adsorbed to the surfaces of gold nanoparticles [23]. This is because there is an interaction between the atom containing the lone pair of electrons and the positive state of the surface of the gold nanoparticle. Therefore, in our study, based on the same principle, the hydroxyl (-OH) in RAC can be adsorbed onto the surfaces of gold nanoparticles [24–26] to achieve the signal enhancement. Additionally, the RAC aptamers coated on the self-assembled film can only recognize RAC so that the other several organic compounds with -NH or -OH groups will not interfere with the selectivity of the biosensor. As a result, we proposed a novel method for RAC detection of high sensitivity and good selectivity by using optical images of liquid crystals based on the gold nanoparticles.

Materials and methods

Chemicals and reagents

The RAC aptamer was obtained from Sangon Biotech Co., Ltd. (Shanghai, China, www.sangon.com). RAC aptamer [5′-NH_2-$(CH_2)_6$-ACGCAGTGCGGGCGA-3′] (reported by Dr. Yao [27]) was synthesized by Sangon Biotech Co., Ltd. (Shanghai, China, www.sangon.com). Silane coupling agent (3-aminopropyl)triethoxysilane (APTES), N,N-dimethyl-N-(3-(trimethoxysilyl)propyl)-1-octadecanaminiuchloride (DMOAP) were provided by Sigma-Aldrich (St. Louis, USA, www.sigmaaldrich.com). Glutaraldehyde (GA) was obtained from Sinopharm Chemical Reagent Co., Ltd. (Shanghai, China, www.sinoreagent.com). LC 4-cyano-4′-pentylbiphenyl (5CB) was purchased from Huajing Scientific and Technological Development Co., Ltd. (Hebei, China, http://hebeihuajinghb.ce.c-c.com/). Copper grid (150 mesh, 20 μm in thickness) was obtained from Beijing Zhongjingkeyi Technology Co., Ltd. (Beijing, China, www.emcn.com.cn). Glass slides were provided by Xinhua Laboratory Glassware Company (Haimen, China, www.xhyq.net). RAC (Germany, Dr. Ehrenstorfer) was provided by Chongqing huierli biotechnology Co., Ltd. Dopamine hydrochloride, terbutaline sulfate, albuterol sulfate and penicillin were purchased from Beijing solarbio technology Co., Ltd. (Beijing, China, www.solarbio.com). AuNPs (10~20 nm, 0.1 $g \cdot L^{-1}$ (500 $\mu mol \cdot L^{-1}$), No:XFJ15) were provided by Nanjing Xianfengnano material technology Co., Ltd. (Nanjing, China, www.xfnano.com). The solutions and buffers used in our work were as follows: aptamer buffer (20 mM Tris-HCl, 10 mM $MgCl_2$, pH = 7.4), aptamer cleaning buffer (2 × SSC containing 0.01% (*v*/v) SDS, pH = 7.0). All the other reagents were of analytical grade. All solutions were prepared with ultrapure water from a purification system (Ulupure, China, www.ulupure.jdzj.com).

Slides preparation of the liquid crystal (LC) aptasensor

The glass slides were first cut into size of 2 cm × 2 cm square. To clean the surface, glass slides were then immersed in freshly piranha solution (70% H_2SO_4, 30% H_2O_2, v/v) at 80 °C for 1 h to remove all organic contaminants. After that, the glass slides were rinsed thoroughly with anhydrous ethanol and deionized water in turn for at least four or five times, drying under the nitrogen and heating at 110 °C for 3 h. The cleaned glass slides were decorated to the DMOAP-coated glass slides and then used as top slides (Fig. S1A) in the LC aptasensor. The cleaned glass slides were also decorated to the RAC aptamers modified glass slides and then served as bottom slides (Fig. S1B) in the LC aptasensor. The detailed preparations of the decorated glass slides were in the ESM (Electronic Supplementary Materials).

Preparation of AuNP-RAC mixtures

The AuNPs-RAC mixed solutions were made into a series of gradient concentrations. Briefly, RAC of different concentrations were immersed in colloidal gold solvents to be prepared into the desired AuNPs-RAC mixed solutions. The AuNPs-RAC mixed solutions stored at 4 °C for next experiments.

Preparation of copper grids

The copper grids (150 mesh, 20 μm in thickness) were immersed in absolute ethanol with ultrasonic wash for 3 min, rinsed with absolute ethanol and deionized water, dried under nitrogen, and then heated at 60 °C for 1 h. The copper grids were for subsequent experiments. The role of copper mesh is to control the liquid crystal thickness and provide proper space for the LC molecules.

Fabrication of LC aptasensor and optical measurement

For the fabrication of the LC aptasensor, 200 μL AuNPs-RAC mixed solution was dropped onto the RAC aptamer modified glass slide at RT for 1 h, then rinsed with plenty of ultrapure water, dried under tiny flow of N_2. After that, a copper grid was placed on AuNPs-RAC-aptamer conjugate coated glass slide, 2 μL of the 5CB was then dropped on the copper grid and a DMOAP-decorated glass slide was placed onto it. At last, two decorated glass slides sandwiched a copper grid and LCs were held together with three binder clips (Fig. S1C).

The optical appearance of the fabricated LC aptasensor was used for RAC detection by using a polarized light microscope (XP-201POL, Changfang, Shanghai, China). Micrographs were obtained with a digital camera (Cannon A640, Japan) mounted on the polarized light microscope.

Spectrophotometer measurements and TEM measurements

To examine the characteristics of the AuNPs-RAC mixture, different concentrations of AuNPs-RAC solutions were analyzed by the spectrophotometer (Multiskan GO-1510, Thermo Fisher, Finland) and TEM (Transmission Electron Microscope Hitachi-7500, Japan) measurement.

Atomic field microscopy (AFM) measurements

To analyze the surface topography of the LC aptasensor films, the AFM images were performed by a SPM-9700 scanning probe microscope (Shimadzu, Japan). In detail, the aptamer-coated glass slide, the RAC (without AuNPs) immobilized glass slide and RAC-AuNPs decorated glass slide were characterized using AFM, respectively.

Result and discussion

Principle of gold nanoparticle-based signal enhancement detection of RAC using optical image of liquid crystals

The basic strategy of gold nanoparticle-based LC aptasenser for sensitive RAC detection is illustrated in Scheme 1. Firstly,

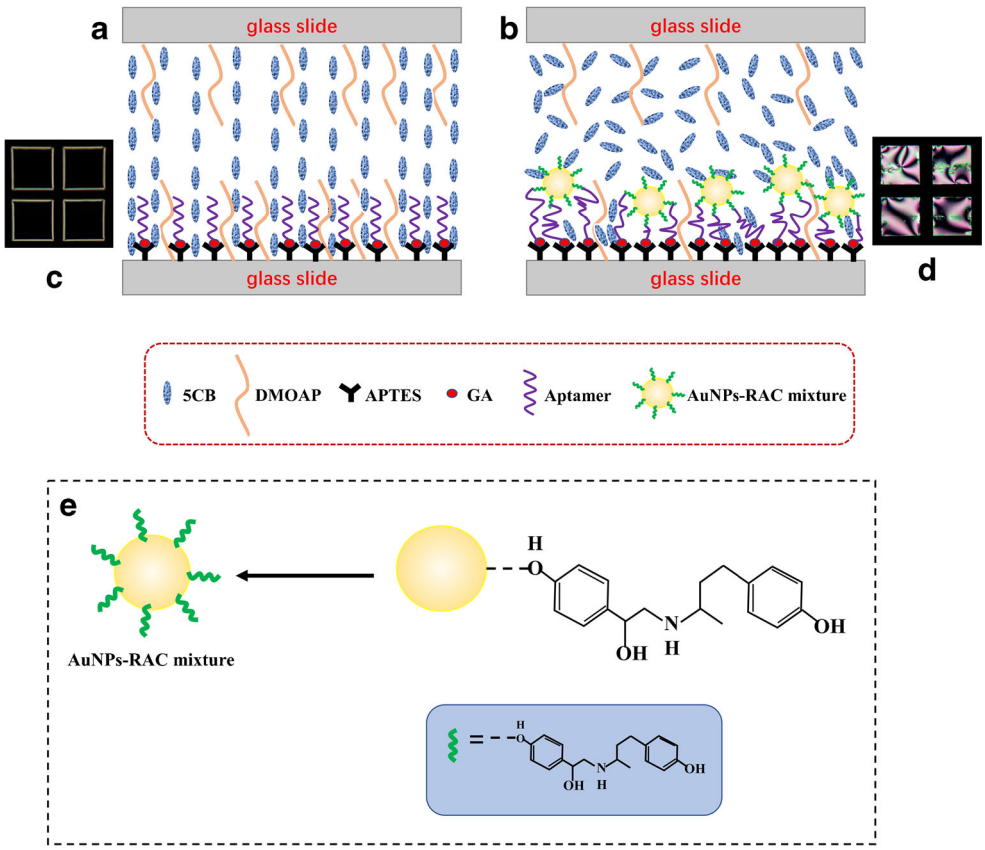

Scheme 1 The schematic illustration of the assay for RAC detection. (**a**) Immobilization of appropriate amount of RAC aptamers on GA/DMOAP-coated glass slides; (**b**) addition of AuNPs-RAC mixtures on the RAC aptamer coated film and the Aptamer-RAC-AuNPs conjugates formed on the substrate surface of the biosensor; (**c**), (**d**) the corresponding polarized images of LCs for (**a**) and (**b**), respectively; (**e**) schematic diagram of the interaction between RAC and AuNPs.

in Sch. 1a, the (APTES+GA)/DMOAP mixed self-assembly films are immobilized onto the glass slides. GA molecules can provide the aldehyde groups to immobilize the RAC aptamers (decorated with amidogen on the 5′ end). The APTES molecules can form covalent Si-O-Si bonds on the surface of the cleaned glass slide. The DMOAP molecules assume homeotropic orientations of the LCs on the glass surface [17]. The appropriate amount of RAC aptamers are decorated on this self-assembly film which do not disrupt the homeotropic orientation of the LCs (Sch. 1a), and the corresponding polarized image is dark (Sch. 1c). Secondly, RAC can be adsorbed to the AuNPs by the interaction between AuNPs and RAC [24–26] to form AuNPs-RAC mixtures, as shown in Sch. 1e. Lastly, the mechanism for orientation behavior of LCs on the substrate surface coated with the Aptamer-AuNPs-RAC conjugates is shown in Sch. 1b. RAC aptamers modified on the substrate can only bind specifically to RAC. Therefore, in the presence of RAC, the aptamer recognized RAC to form the Aptamer-AuNPs-RAC conjugates, which remarkably destroyed the homeotropic orientations of the LCs. As a result, the corresponding polarized images of the LCs change from dark to color (Sch. 1d).

Optimal conditions

The orientation of LC molecules is sensitive to the minute changes of a bounding interface within 100 μm [28]. Excessive amounts of aptamers will disrupt the homeotropic orientation of LCs. However, too few aptamers will reduce the sensitivity of the aptasensor. Herein, to ensure the homeotropic orientation of the LC molecules and facilitate the following detection for RAC, the optimal concentration of aptamers must assume "stand up" orientation on the GA/DMOAP-coated glass slides. As we know, when the LCs are of a homeotropic arrangement, light will not pass through the crossed analyzer and result in a dark polarized image. In contrast, when the homeotropic arrangement of the LCs is disrupted, the light will go through. Then some light will pass through the analyzer, resulting in a bright and color optical appearance of LCs [29]. As shown in Fig. S2, the polarized images of the LCs change from color to dark when the concentrations of RAC aptamers decrease from 500 nM to 50 nM. A uniformly homeotropic orientation of LCs can ensure the detection accuracy of the aptasensor. Consequently, we

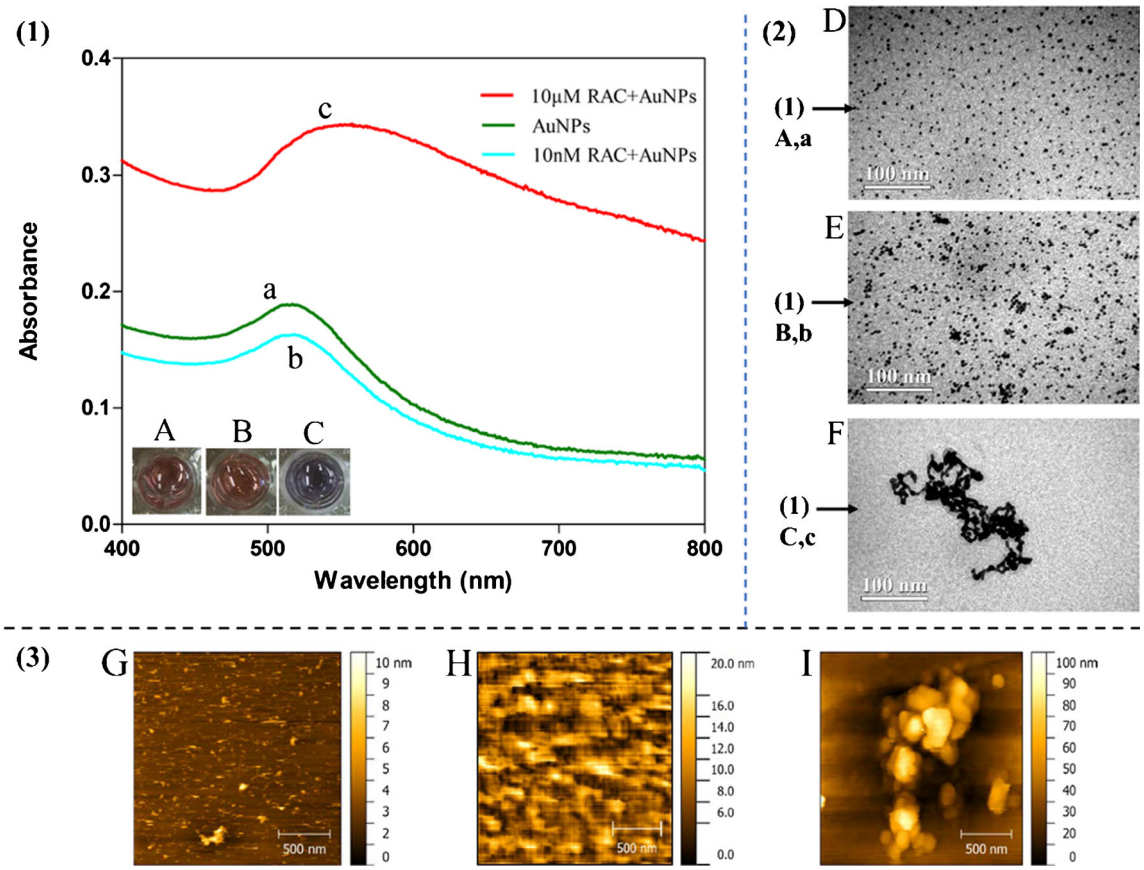

Fig. 1 (1) The absorption spectrograms and the optical photos of actual samples of the AuNPs-RAC mixed solutions at the different concentrations of RAC: (a, A) 0 pM, (b, B) 10 nM and (c, C) 10 μM; (2) The corresponding TEM images of the AuNPs-RAC mixed solutions at the different concentrations of RAC: (D) 0 pM, (E) 10 nM and (F) 10 μM; (3) AFM results of surfaces modified with (G) aptamers (100 nM), (H) RAC (10 nM) and (I) AuNPs-RAC mixtures (10 nM)

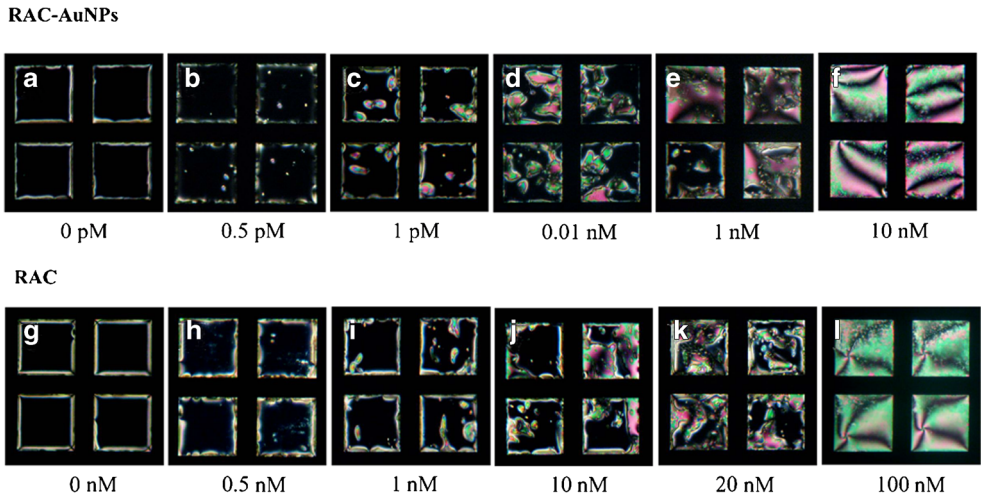

Fig. 2 The polarized images of LCs for RAC-AuNPs at different RAC concentrations: (**a**) 0 pM, (**b**) 0.5 pM, (**c**) 1 pM, (**d**) 0.01 nM, (**e**) 1 nM, (**f**) 10 nM; and the polarized images of LCs for only RAC at different concentrations: (**g**) 0 nM, (**h**) 0.5 nM, (**i**) 1 nM, (**j**) 10 nM, (**k**) 20 nM, (**l**) 100 nM

infer that the appropriate amount of RAC aptamers immobilized on the LC aptasensor is 100 nM (Fig. S2E).

In this assay, the characteristics of AuNPs-RAC mixed solution were first investigated by the spectrophotometer. The pure AuNPs without any RAC (0 pM), AuNPs-RAC mixed solution at the RAC concentrations of 10 nM and 10 μM were chosen as the different samples respectively. The scanning results of the absorption spectra for different samples are shown in Fig. 1(1). The corresponding wavelengths of the maximum peaks of absorption for the three different samples are 513 nm (Fig. 1(1)a), 517 nm (Fig. 1(1)b) and 542 nm (Fig. 1(1)c), respectively. Then their corresponding particle sizes were calculated from eq. (1) [26, 30]. The particle size of AuNPs without any RAC was about 10 nm, and 10 nM of AuNPs-RAC mixture was about 16 nm, which was the result of RAC adsorbed onto the AuNPs. It has been proved that different absorption spectrum peaks correspond to different sizes of nanoparticles [31]. Hence, as the RAC concentration increased, the particle size of the AuNPs-RAC mixture increased. Especially when the concentration of RAC is 10 μM, there is a clear red shift in the maximum absorption peak (Fig. 1(1)c). This result can also be confirmed by observing the color of the mixtures visually, as shown in Fig. 1(1)A, B, C.

$$\lambda_{max} = 507.1 + 8.68 \times \ln[0.2 \times \text{size(AuNPs)(nm)}] \quad (1)$$

λ_{max} : absorption peak.

The adsorption between AuNPs and RAC was also verified with TEM (Transmission Electron Microscopy). Figure 1(2) shows the TEM images of pure AuNPs (Fig. 1(2)D), 10 nM of AuNPs–RAC mixture (Fig. 1(2)E) and 10 μM of AuNPs–RAC mixture (Fig. 1(2)F). By comparing Fig. 1(2)D, E, we can find out that when RAC of 10 nM was mixed with AuNPs, the RAC-AuNPs mixture had a bigger particle size than pure AuNPs. Furthermore, apparent reunion occurred when RAC of 10 μM was blended with AuNPs, as deduced from the TEM image (Fig. 1(2)F). Compared with AuNPs, AuNPs–RAC mixture possesses a brighter aura and a bigger particle size. These phenomena confirmed that RAC was adsorbed to the AuNPs.

To investigate the LC aptasensor substrate surface decorated with different molecules, AFM scanning was performed for the study. AFM results are shown in Fig. 1(3). Previous results have manifested that ss-DNA molecules are globular, while short ds-DNA molecules are generally rod-like in shape [17, 32]. Therefore, as shown in Fig. 1(3)G, we infer that the aptamers coated on the glass slide without binding RAC did not form similar ds-DNA structures by themselves because the AFM result (Fig. 1(3)G) shows globular structures in the image. Specific binding of aptamers to RAC greatly changed the substrate topography (Fig. 1(3)H, I). Furthermore, comparing Fig. 1(3)H with Fig. 1(3)I, it can be concluded that RAC was adsorbed to the AuNPs. Because if RAC was not adsorbed onto the AuNPs, there will be no differences between Fig. 1(3)H, I.

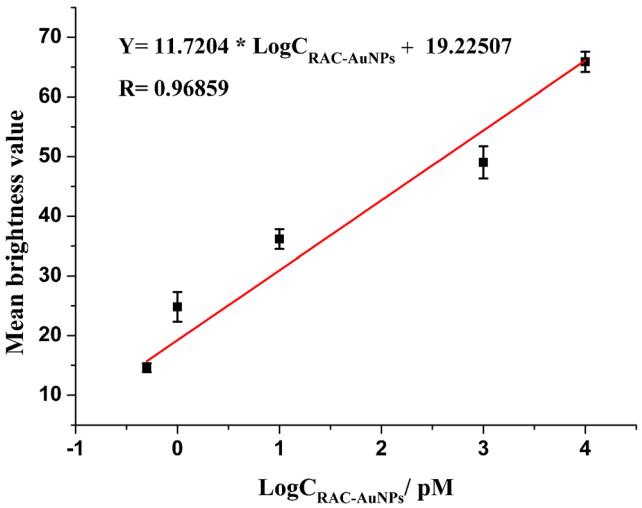

Fig. 3 Calibration plot of the mean brightness value of the polarized image vs the logarithm of RAC-AuNPs concentration (Y is the mean brightness value of the polarized image, $C_{RAC\text{-}AuNPs}$ is the concentration of RAC-AuNPs, $n = 3$)

Table 1 Comparison with currently available methods for the detection of RAC

Method of detection	Limit of detection	References
Colorimetric method	0.22 μmol·L^{-1}	[33]
Electrochemiluminescence (ECL) immunosensor	2.6 pg·mL^{-1}	[34]
Gas chromatography–mass spectrometry	3.6 ng·g^{-1} (4.28 ng·mL^{-1})	[6]
Liquid chromatography-mass spectrometry	0.4 ng·g^{-1} (0.48 ng·mL^{-1})	[7]
Immunoassay	2.5 pg·mL^{-1}	[10]
Chemiluminescence	0.5 ng·mL^{-1}	[12]
AuNP-based liquid crystal aptasensor	1 pmol·L^{-1} (0.3 pg·mL^{-1})	This work

Detection sensitivity

With these optimal conditions, the aptamer-AuNP-based LC biosensor was performed to realize the detection of RAC. The polarized images of LCs for RAC-AuNPs mixtures at different RAC concentrations are exhibited in Fig. 2a-f. The polarized images of LCs are dark in the absence of RAC (Fig. 2a). The results demonstrated that aptamers did not react with AuNPs and the AuNPs did not interfere with the detection results. We inferred that it was due to that the aptamers had been vertically modified onto the substrate surface rather than being in a free crimp state. When the concentration of RAC-AuNPs increased from 0.5 pM to 10 nM (Fig. 2b-f), the birefringent textures in the polarized images were intensified, showing that the detection limit of this assay is as low as 1 pM (Fig. 2c), which benefited from both the large surface areas of the gold nanoparticles and the high sensitivity of LC molecules to the minute changes of the substrate surface. As shown in Fig. 2c-f, the bright and color areas grow larger constantly as the RAC concentration increased, suggesting that a greater number of Aptamer-AuNPs-RAC conjugates were presented on the surface to destroy the orientational profile of LCs.

To confirm the gold nanoparticles can indeed improve the detection sensitivity, the AuNPs-RAC mixture solutions were replaced by RAC solutions. The polarized images of the only RAC detection results are shown in Fig. 2g-l. It can be certified that the detection sensitivity by using AuNPs is a great deal higher than that without AuNPs. Through the use of gold nanoparticles, that interact with RAC, a significant signal enhancement is achieved.

As indicated in Fig. 3, the calibration curve showed approximate linear relationship between the mean brightness value of the polarized image and the logarithm of RAC-AuNPs concentration in the range from 0.5 pM to 10 nM. This method has a satisfactory detection limit of 1 pM for RAC. Notably, the sensitivity of this method is higher than those of reported methods (Table.1). As shown in Table 1, the proposed lowest detection limit for RAC assay (2.5 pg·mL^{-1}) was about 8 times higher than our detection limit

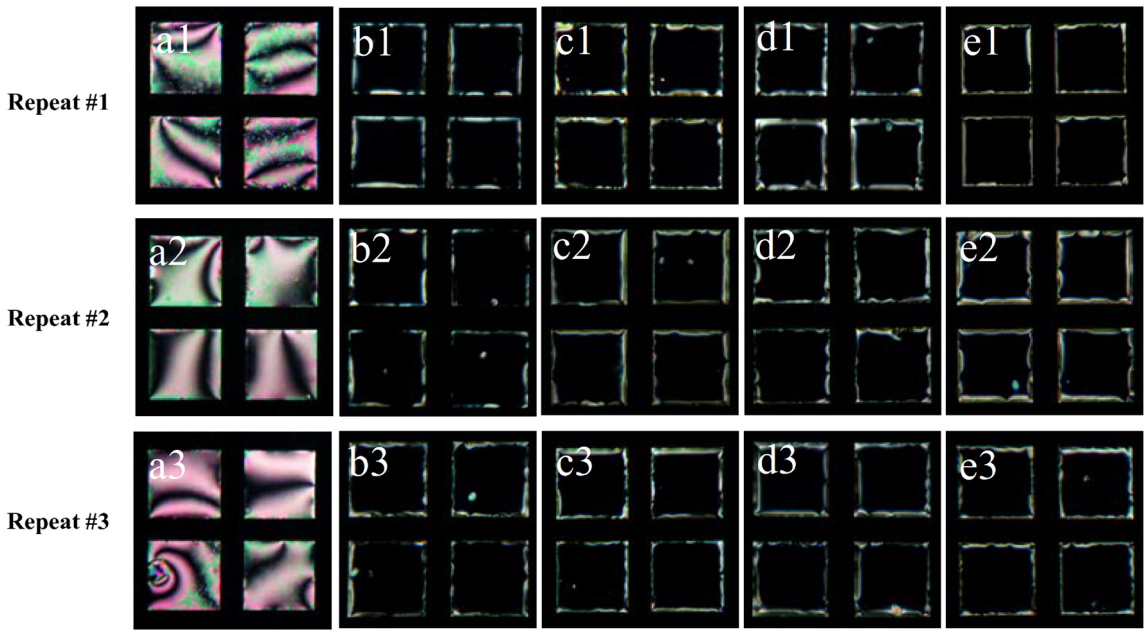

Fig. 4 Selectivity and reproducibility of AuNP-based LC aptasensor to (a1, a2, a3) RAC (10 nM), (b1, b2, b3) dopamine hydrochloride (10 nM), (c1, c2, c3) terbutaline sulfate (10 nM), (d1, d2, d3) albuterol sulfate (10 nM), (e1, e2, e3) ampicillin (10 nM)

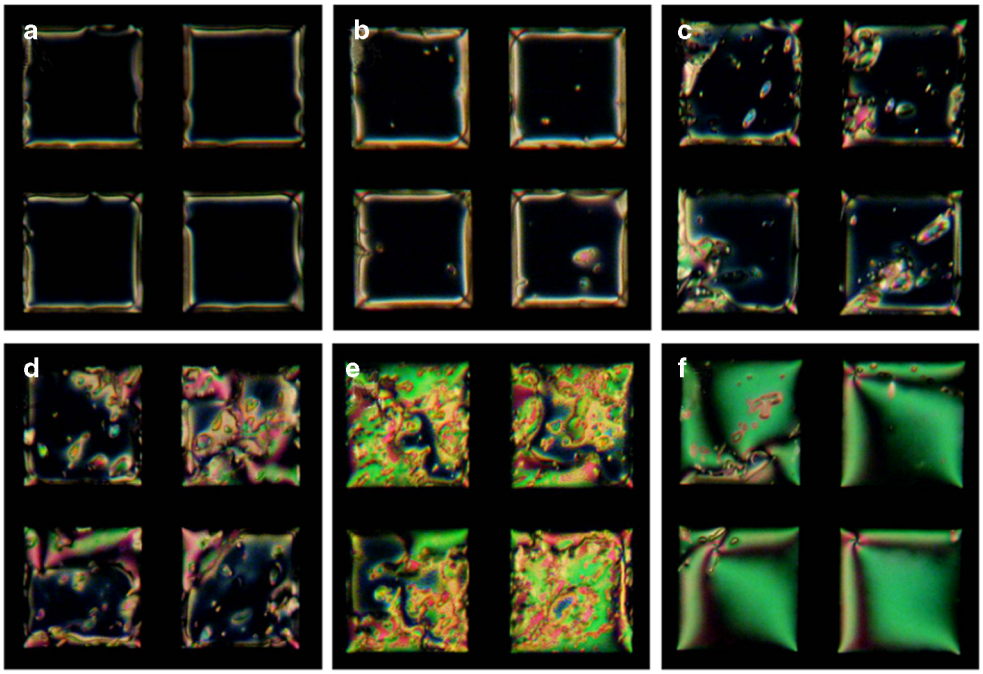

Fig. 5 The polarized images of LCs for RAC-AuNPs mixtures in real samples at different RAC concentrations: (**a**) 0 pM, (**b**) 0.5 pM, (**c**) 1 pM, (**d**) 0.01 nM, (**e**) 1 nM, (**f**) 10 nM

(1 pmol·L^{-1}). The high sensitivity of this assay may be ascribed to both the nanoparticles and the efficient domino effect of the LC molecules.

Detection selectivity and reproducibility

Lastly, the selectivity and the reproducibility of the LC assay were evaluated by replacing with relevant interfering agents that had the similar structures with RAC and were difficult to distinguish. The interfering agents were also made into mixture solutions by blending with AuNPs. The interfering agents were dopamine hydrochloride, terbutaline sulfate, albuterol sulfate and ampicillin, respectively. The polarized images of these interferents are exhibited in Fig. 4. As shown in Fig. 4B1-E1(Repeat #1), the polarized images of LCs are dark with few bright spots, while most of the images show a uniform dark background. This approach also has a good reproducibility, as confirmed in Fig. 4 b2-e2 (Repeat #2) and Fig. 4 b3-e3 (Repeat #3). Results indicated that there were not obvious differences in the control groups, because the interfering agents cannot be recognized specially by the RAC aptamer to form Aptamer-RAC-AuNPs conjugates. For RAC-AuNPs groups, the situation was just reversed, and the birefringent textures in the polarized images were clearly visible (Fig. 4 a1, a2, a3). Hence, this approach possesses a good detection selectivity and reproducibility.

Real sample analysis

The International Olympic Committee has introduced policies that prohibit the use of β2 agonists such as clenbuterol and stimulants. Therefore, detection of RAC residues in human urine is also significant. To further evaluate the practical performance of the sensing system for detecting real samples, the human urine samples were firstly diluted 10 times by ultrapure water to yield testing sample solutions. And then, AuNPs-RAC mixtures at different RAC concentrations (0 pM, 0.5 pM, 1 pM, 0.01 nM, 1 nM and 10 nM) were spiked into the diluted testing samples, respectively. As shown in Fig. 5, the detection results for real samples were the same as the detection results in ultrapure water. As the concentration increased from 1 pM to 10 nM (Fig. 5c-f), the birefringent textures in the polarized images were intensified. While when the concentration of real sample was 0 pM, the polarized image shows a full dark optical appearance (Fig. 5a), which indicated that the AuNPs in real samples didn't bring interference to the detection results. The real sample analysis suggested that this new method for RAC detection was reliable and feasible.

Conclusions

We have developed a new LC aptasensor for sensitive and selective detection of RAC based on AuNPs. AuNPs used in this study can remarkably improve the performance of the LC aptasensor. With AuNPs, this method owns the detection scope in the range from 1 pM to 10 nM. This method also has some limitations. There is still a lot of work to do on the quantitative detection of the LC biosensor. Our group will further improve the application of this method in actual sample detection. The detection results can be easily observed

visually through a crossed polarizer. This method is superior to the reported methods for RAC assay.

Acknowledgements This work is financially supported by the Doctoral Research Startup Foundation of Jining Medical University, the Natural Science Foundation of Chongqing (CSTC2015JCYJA20014) and Ministry of Education (CQKLBST-2515005).

Compliance with ethical standards

Conflict of interest The authors declare that they have no conflict of interest.

References

1. Crescenzi C, Bayoudh S, Cormack PAG, Klein T, Ensing K (2001) Determination of Clenbuterol in bovine liver by combining matrix solid-phase dispersion and molecularly imprinted solid-phase extraction followed by liquid chromatography/electrospray ion trap multiple-stage mass spectrometry. Anal Chem 73(10):2171–2177
2. Shishani E, Chai SC, Jamokha S, Aznar G, Hoffman MK (2003) Determination of ractopamine in animal tissues by liquid chromatography-fluorescence and liquid chromatography/tandem mass spectrometry. Anal Chim Acta 483(1–2):137–145
3. Rajkumar M, Li YS, Chen SM (2013) Electrochemical detection of toxic ractopamine and salbutamol in pig meat and human urine samples by using poly taurine/zirconia nanoparticles modified electrodes. Colloids Surf, B 110(10):242–247
4. Yao X, Yan P, Tang Q, Deng A, Li J (2013) Quantum dots based electrochemiluminescent immunosensor by coupling enzymatic amplification for ultrasensitive detection of clenbuterol. Anal Chim Acta 798(18):82–88
5. Noel JA, Barstow TJ, Broxterman RM, McCoy GD, Phelps KJ, Gonzalez JM (2016) Effect of Ractopamine-HCL on muscle fiber types and finishing barrow exhaustion. Meat Sci 112:110
6. Ye D, Wu S, Xu J, Jiang R, Zhu F, Ouyang G (2016) Rapid determination of Clenbuterol in pork by direct immersion solid-phase microextraction coupled with gas chromatography-mass spectrometry. J Chromatogr Sci 54(2):112–118
7. Li J, Chen Y, Su YQ, Ding XM, Xia WS, Liu HM, Zhang YB (2017) Single-step multiresidue determination of β-lactam antibiotics and β-agonists in porcine muscle by liquid chromatography-tandem mass spectrometry. Food Anal Methods 10:2185–2193
8. Chu L, Zheng S, Qu B, Geng S, Kang X (2017) Detection of β-agonists in pork tissue with novel electrospun nanofibers-based solid-phase extraction followed ultra-high performance liquid chromatography/tandem mass spectrometry. Food Chem 227: 315–321
9. Lin YP, Lee YL, Hung CY, Huang WJ, Lin SC (2017) Determination of multiresidue analysis of β-agonists in muscle and viscera using liquid chromatograph/tandem mass spectrometry with quick, easy, cheap, effective, rugged, and safe methodologies. J Food Drug Anal 25(2):275–284
10. Zhang Y, Ma H, Wu D, Li Y, Du B, Wei Q (2015) Label-free immunosensor based on au@ag 2 S nanoparticles/magnetic chitosan matrix for sensitive determination of ractopamine. J Electroanal Chem 184:3765–3771
11. Wang WY, Zhang YL, Wang JY, Xue S, Ye JN (2010) Determination of β-agonists in pig feed, pig urine and pig liver using capillary electrophoresis with electrochemical detection. Meat Sci 85(2):302–305
12. Han J, Gao H, Wang W, Wang Z, Fu Z (2013) Time-resolved chemiluminescence strategy for multiplexed immunoassay of clenbuterol and ractopamine. Biosens Bioelectron 48(19):39–42
13. Brake JM, Abbott NL (2003) Biomolecular interactions at phospholipid-decorated surfaces of liquid crystals. Science 302(5653):2094–2097
14. Kim SR, Shah RR, Abbott NL (2000) Orientations of liquid crystals on mechanically rubbed films of bovine serum albumin: a possible substrate for biomolecular assays based on liquid crystals. Anal Chem 72(19):4646–4653
15. Mcumber AC, Noonan PS, Schwartz DK (2012) Surfactant-DNA interactions at the liquid crystal-aqueous interface. Soft Matter 8(16):4335–4342
16. Li X, Tan H, Li Y-L, Wu Z-Y, Shen GL, Yu R-Q (2014) Aptamer-based liquid crystal biosensor for detection of platelet-derived growth factor BB. Chinese J Anal Chem 42(5):629–635
17. Wang Y, Wang B, Shen J, Xiong XL, Deng SX (2017) Aptamer based bare eye detection of kanamycin by using a liquid crystal film on a glass support. Microchim Acta:1):1–1):7
18. Wu Y, Wu C, Shen S, Yu Z, Ruqin G (2013) Split Aptamer-Based Liquid Crystal Biosensor for ATP Assay. Acta Chim Sin 71(3):367
19. Yuan Q, Lu D, Zhang X, Chen Z, Tan W (2012) Aptamer-conjugated optical nanomaterials for bioanalysis. TrAC Trends Anal Chem 39:72–86
20. Cao YC, Jin R, Mirkin CA (2002) Nanoparticles with Raman spectroscopic fingerprints for DNA and RNA detection. Science 297(5586):1536–1540
21. Lan D, Li B, Zhang Z (2008) Chemiluminescence flow biosensor for glucose based on gold nanoparticle-enhanced activities of glucose oxidase and horseradish peroxidase. Biosens Bioelectron 24(4):940–944
22. Mahyari M, Shaabani A, Behbahani M, Bagheri A (2014) Thiol-functionalized fructose-derived nanoporous carbon as a support for gold nanoparticles and its application for aerobic oxidation of alcohols in water. Appl Organomet Chem 28(8):576–583
23. Grabar KC, Freeman RG, Hommer MB, Natan MJ (1995) Preparation and characterization of au colloid monolayers. Anal Chem 67(4):735–743
24. Kristensen IS, Mowbray DJ, Thygesen KS, Jacobsen KW (2008) Comparative study of anchoring groups for molecular electronics: structure and conductance of au-S-au and au-NH(2)-au junctions. J Phys Condens Matter 20(37):374101
25. Izquierdolorenzo I, Sanchezcortes S, Garciaramos JV (2011) Trace detection ofaminoglutethimide drug by surface-enhanced Raman spectroscopy: a vibrational and adsorption study on gold nanoparticles. Anal Methods 3(7):1540–1545
26. Duan J, He D, Wang W, Liu Y, Wu H, Wang Y, Fu M, Li S (2013) The fabrication of nanochain structure of gold nanoparticles and its application in ractopamine sensing. Talanta 115(17):992–998
27. Yang F, Wang P, Wang R, Zhou Y, Su X, He Y, Shi L, Yao D (2016) Label free electrochemical aptasensor for ultrasensitive detection of ractopamine. Biosens Bioelectron 77:347–352
28. Koenig GM, Abbott NL (2010) Chemoresponsive assemblies of microparticles at liquid crystalline interfaces. Proc Natl Acad Sci U S A 107(9):3998–4003
29. Miller DS, Carlton RJ, Mushenheim PC, Abbott NL (2013) Instructional review: an introduction to optical methods for characterizing liquid crystals at interfaces. Langmuir 29(10):3154–3169
30. Song HY, Kang TF, Li NN, Lu LP, Cheng SY (2016) Highly sensitive voltammetric determination of kanamycin based on aptamer sensor for signal amplification. Anal Methods 8(16):3366–3372
31. Peng Y, Li L, Mu X, Guo L (2013) Aptamer-gold nanoparticle-based colorimetric assay for the sensitive detection of thrombin. Sensors Actuators B Chem 177(1):818–825

32. Hansma HG, Revenko I, Kim K, Laney DE (1996) Atomic force microscopy of long and short double-stranded, single-stranded and triple-stranded nucleic acids. Nucleic Acids Res 24(4):713–720
33. Rohit JV, Kailasa SK (2017) Simple and selective detection of pendimethalin herbicide in water and food samples based on the aggregation of ractopamine-dithiocarbamate functionalized gold nanoparticles. Sensors Actuators B Chem 245:541–550
34. Zhu Q, Liu H, Zhang J, Wu K, Deng A, Li J (2017) Ultrasensitive QDs based electrochemiluminescent immunosensor for detecting ractopamine using AuNPs and au nanoparticles@PDDA-graphene as amplifier. Sensors Actuators B Chem 243:121–129